Title

Simulating the Potential for Invasive Grass Expansion to Alter Wildfire Behavior in Southern California with WRF-Fire

Author

Wang, Bowen

Publication Date

2024

Peer reviewed|Thesis/dissertation

UNIVERSITY OF CALIFORNIA

Los Angeles

Simulating the Potential for Invasive Grass Expansion to Alter Wildfire Behavior in Southern California with WRF-Fire

A thesis submitted in partial satisfaction

of the requirements for the degree Master of Arts

in Geography

by

Bowen Wang

2024

ABSTRACT OF THE THESIS

Simulating the Potential for Invasive Grass Expansion to Alter Wildfire Behavior in Southern California with WRF-Fire

by

Bowen Wang

Master of Arts in Geography

University of California, Los Angeles, 2024

Professor Park Williams, Chair

Abstract

Invasion by non-native annual grasses poses a serious threat to native vegetation in California, and interference with native ecosystems may be facilitated through interaction with wildfires. Our work is the first attempt to use the coupled fire-atmosphere model, WRF-Fire, to investigate how shifts from native, shrub-dominated vegetation to invasive grasses could have affected a known wildfire event in southern California. We simulate the Mountain Fire, which burned >11,000 ha in July 2013, under idealized fuel conditions that represent varying extents of grass invasion. Expanding grass to double its observed coverage causes fire to intensify and spread faster due to increased wind speed. Beyond this, further grass expansion reduces the simulated spread rate and intensity because the relatively low fuel loads of grasses partially offset the positive wind-speed effect. Overall, our simulations suggest that grass expansion would generally promote larger, faster spreading wildfires in southern California, motivating continued efforts to reduce the spread of invasive annual grasses in this region.

The thesis of Bowen Wang is approved.

Alexander D. Hall

Dennis P. Lettenmaier

Park Williams, Committee Chair

University of California, Los Angeles

2024

Table of Contents

Table of Figures

Supplementary Figure 8. Comparison of the raw NIFC fire perimeter at 6:45 am, July 16th and the final fire perimeter. The observed perimeter at 6:45 am, July 16th erroneously covers a portion of the area beyond the fire's final perimeter. Thus, the perimeter shown in **Figure 2a** has the perimeter cropped so that it only covers the area within the final fire perimeter.

Supplementary Figure 9. Fire perimeters ~17 hours after ignition under all 8 scenarios overlaid on their respective fuel conditions.

Supplementary Figure 10. U-component wind at ~7 hours after ignition near the fire perimeter. The wind is westerly throughout the demonstrated area. A positive (negative) change indicates a stronger (weaker) westerly wind.

Supplementary Figure 11. 60-minute rolling mean of the **(a, c)** total and **(b, d)** area-averaged WRF-Fire simulated fire radiative power (FRP) under **(a, b)** Scenarios A to D and **(c, d)** Scenarios D to E. The high FRP in Scenarios C_1 and D is consistent with their fastest fire spreads.

Acknowledgments

I'd like to express my most sincere gratitude to my thesis advisor, Park Williams, for his support and mentorship in the last year and a half. His attention to detail, emphasis on creativity, and passion for science have profoundly shaped my development as a researcher. What I look up to him the most is his kindness, patience, and humility. He always makes himself available to students, even when he is already extremely busy. Park is a constant inspiration for me to become a better person.

I also have the honor to have worked with Dr. Alex Hall in the AOS department for three years. I deeply appreciate Alex's mentorship, patience, and the freedom he gave me in doing research, all of which allowed me to learn, grow, and eventually become a better researcher. Alex also cordially invited and convinced me to work with the group for all three summers since I joined the group. Those summers turned into times when I grew the most.

Alex also assembled a phenomenal research group - the UCLA Center for Climate Science - from which I have learned tremendously. I will always be proud to have been a part of the group. I want to give a special thank you to Ben Bass for leading me into the doors of research. I certainly would not have reached where I am without Ben's mentorship. Gavin Madakumbura has now become one of my closest friends. I truly enjoyed chatting with him, when I learned so much about both research and random facts in academia. I thank Chad Thackrey and Jesse Norris for the happy hour beers and chats at Broxton. Thank you also to Stefan Rahimi, Eli Dennis, Surabhi Biyani, Stephen Croppers, Sara Graves, Will Krantz, Emily Slinskey, Lei Huang, and Elease Lui Stemp.

I also want to give a huge thanks to everyone in the HyFiVeS research group for their friendship and support. It has been a great pleasure to have shared office space with Jacob Jones,

Melissa Ferriter, Qian He, Miriam Johnston, and Matt Dannenberg. They are the reason why I go to the office, and I will certainly miss all the times that we spent with each other. A special thank you to Miriam for her kindness, guidance, and generosity with her time throughout my grad school application process. I didn't get to spend as much time with Ari Varuolo-Clarke and Caroline Juang at Columbia University, but I always enjoyed my time with them when we met.

My friends both at UCLA and beyond are an integral part of what makes this journey special. Playing ultimate frisbee has been an important element of my time at UCLA. I want to thank especially Zepeng (Jeffrey) Yu, Muyuan (Nicole) Xu, Jingyi (Thea) Huang, Xuyang (Nick) Zhou, Weizhi (Amanda) Gong, Zunhong (Quentin) Mei, and Yueshan (Shade) Wang. My special thanks goes to Jeffrey, with whom I have developed unparalleled chemistry in both frisbee and basketball. His timely deep throws and our pick-and-roll and dribble handoff plays are what bring joy to playing sports. I also want to thank my middle/high school friends at Beijing National Day School, especially Muchen Li, Jiajun Lu, Kewei Cao, Dinghui Chen, Zihan Zhou, Boran Zhang, Xuan Zhou, Xiangyue Que, Luehan Wang, and many others. The journey wouldn't have been complete without their friendship.

I would like to give my heartfelt thank you to my girlfriend Yue Ma for the joy and love she brought to my life in the last four years. Her presence and support have been integral to my college life. And finally, I want to thank my parents, Yan Zhang and Yuxiang Wang, for their unwavering support and for making all this possible.

1 Introduction

Invasion by non-native annual grasses seriously threatens native vegetation in California (Corbin and D'Antonio, 2004; Sandel and Dangremond, 2012; Bradley et al., 2018; Smith et al., 2022). Through interactions between invasive annual grasses and wildfires known as the grass-fire cycle (D'Antonio, 1992), invasions change both local vegetation landscapes and wildfire regimes (Abatzoglou & Kolden, 2011; Brooks et al., 2004), and wildfires have the potential to increase the spread of invasive plants (Rew & Johnson, 2010; Abatzoglou & Kolden, 2011). This occurs if invasive species can recover faster than natives and outcompete natives for water and nutrients (D'Antonio, 1992; Mordecai et al., 2015; Donovan et al., 2023). The expansion of invasive annual grasses may subsequently promote fire spread (Balch et al., 2013; Fusco et al., 2019; Smith et al., 2023) if they increase fine fuel loads and connectivity and/or dry out faster than native vegetation (Davies and Nafus, 2013).

Investigations into how invasive grasses affect wildfire have demonstrated that areas dominated by invasive grasses tend to be more fire-prone. For example, even small amounts of invasive annual grasses like cheatgrass (*Bromus tectorum*) can increase fire frequency in an ecosystem (Bradley et al., 2018). Invasive grasses are also more likely to promote longer and larger wildfires (Balch et al., 2013). While these statistical relationships provide important information on the impacts of invasive grass expansion, they cannot control for the various environmental factors (e.g., climate, weather, and vegetation conditions) that may confound the results. Few studies have modeled how a known fire event of interest woudl have been affected by invasive grass expansion. To our knowledge, the only study that has attempted to address a similar question is Tortorelli et al. (2023), who used a statistical fire simulator to model how fire probabilities and sizes would change under a hypothetical vegetation condition with more

invasive grasses in the Blue Mountains ecoregion in the Pacific Northwest. However, we know of no existing literature on how the behaviors of a particular wildfire event would have been affected by a hypothetical fuel condition where the abundance of invasive plants is modified.

This study aims to fill this gap using a dynamical modeling approach to investigate how shifts in southern Californian vegetation, particularly from native species to invasive grasses, would affect wildfire behavior. We use the state-of-the-art Weather and Research Forecasting (WRF) model (Skamarock et al., 2019), coupled with a wildland fire behavior module (WRF-Fire; Coen et al., 2013). WRF-Fire has been used to simulate wildfire events (e.g., Shamsaei et al., 2023; Juliano et al., 2024; DeCastro et al., 2022) and how they may be affected by fuel properties like fuel load and fuel moisture content (e.g., Turney et al., 2023; Roberts et al., 2023). However, to our knowledge, our work is the first to use WRF-Fire to examine how changes in fuel types may alter fire behaviors. To address this question, we consider the 2013 Mountain Fire in southern California, simulating the fire under both an observed fuels scenario and idealized scenarios representing varying extents of annual grass invasion. We seek to understand how an expansion of invasive grasses would change the spread and intensity of the Mountain Fire.

2 Materials and Method

2.1 Case study: Mountain Fire, 2013

To understand how changes in vegetation composition may affect wildfire spread and intensity, we simulate the 2013 Mountain Fire, which occurred primarily on Mt. San Jacinto in the San Bernadino National Forest in Riverside County of southern California. The fire started roughly at 13:45 local time on July 15th, 2013, due to an electrical equipment failure and was contained on July 30th (Cocca, 2013). It burned over about 11141 hectares (**Figure S1**) and

destroyed 23 structures. We select the Mountain Fire because this domain has a favorable climate, topography, and soil conditions for the spread of invasive grass (**Figure S2**; McMahon et al., 2021). The study domain is also in a region where intense wildfire and smoke have the potential to pose significant safety and health risks (Aguilera et al., 2021). The Mountain Fire caused the evacuation of Idyllwild, a small mountain town situated in highly flammable vegetation with few escape routes. Palm Springs is immediately to the east with a population of over 40,000 people, many of whom are elderly and at higher risk of respiratory problems (Lipsett et al., 2006), and the coastal metropolis to the west is also at risk of heavy smoke exposure during fires driven by offshore Santa Ana wind events (Aguilera et al., 2021). Thus, changes in fuel conditions that would act to enlarge and/or intensify a wildfire on Mt. San Jacinto or within the greater region of the San Bernardino Mountains would likely have substantial and diverse negative consequences on numerous populations across southern California.

In this study, we focus on roughly the first day of the Mountain Fire, when the fire spreaded the most rapidly and covered a significant portion of shrubland, which is most susceptible to the invasion of non-native grasses (Davies et al., 2021). The starting period is also when the fire can be most accurately simulated and is least affected by factors like the human construction of containment lines, which can add substantial uncertainties to the fire modeling (Turney et al., 2023).

2.2 Fire modeling: WRF-Fire

We perform our simulations using the coupled fire-atmosphere model WRF-Fire, which is the WRF v4.4 (Skamarock et al., 2019) model coupled with a fire behavior model based on the semi-empirical Rosthermal rate-of-spread (ROS) equations (Coen et al., 2013; Muñoz-Esparza et

al., 2018; Rothermal, 1972). Fire spread is determined primarily by wind speed, terrain slope, and fuel characteristics. By spreading and consuming fuel, the fire releases heat to the atmosphere (i.e., fire radiative power; FRP), which is calculated as a function of ROS and fuel characteristics (Coen et al., 2013). The released heat feeds back to WRF, altering local winds which affect the fire spread.

To drive the WRF model, we use the fifth-generation ECMWF Reanalysis (ERA5; Hersbach et al., 2020) which has a horizontal resolution of 27 km. In WRF, we set up 4 two-way nested domains, with horizontal grid cell spacing of 9 km, 3 km, 600 m, and 120 m, from the outermost to innermost domain, respectively (**Figure S3**). The innermost domain is further refined into 4x4 subgrids of 30 m horizontal spacing for the fire model. Important physics schemes are introduced in **Text S1**.

We acquire topography and fuel category data at 30-m resolution from LANDFIRE (**Figure S4**). In particular, the fuel data is based on the Anderson-13 fuel categories (Anderson-13; Anderson, 1982) from the LANDFIRE 2012 dataset, the last update to the dataset before the Mountain Fire occurred. Anderson-13 is the fuel model applied in the currently publicly available version of WRF-Fire. In our case, it characterizes each 30 m grid cell either as one of the three general fuel types (grass, shrub, and timber) or as no fuel (e.g., roads, urban land, water). We halve the fuel load for all categories since the fuel models tend to overestimate fuel load in the grass- and shrub-dominated categories that encompass the majority of our study site (Tortorelli et al., 2023), although the opposite may be true for forest fires (Roberts et al. 2024; Turney et al., 2023). We also manually adjust the fuel category input to WRF-Fire so that all roads relevant to the fire are represented as continuous stretches of no-fuel grid cells with no gaps in between (**Text S2**, **Figure S5**). We evaluate the model performance by comparing the

fire simulated under the baseline, observed conditions to the observed fire perimeters from the Visible Infrared Imaging Radiometer Suite (VIIRS) and the National Interagency Fire Center (NIFC).

2.3 Alternative fuel conditions

To simulate effects of non-native grass invasion, we develop idealized fuels scenarios, referred to as A–E, by modifying the LANDFIRE Anderson-13 fuel categories maps. Note that while fuel moisture content and its variations across different vegetation types may affect the fire spread, here we primarily focus on the impact of the changing fuel load on fire and assume a constant dead fuel moisture of 8% across the domain. Scenario A uses the observed 2012 Anderson-13 fuels map. Scenarios B–D represent cases where vegetated, but non-grass, grid cells from A are increasingly replaced with grasses. In Scenario B, the grid cells labeled as the grass and understory category (the most abundant type of grass cover in our study area) in Scenario A are allowed to spread and replace any neighboring grid cells categorized as brush. In Scenario C, the grass and understory grid cells in Scenario B spread again to their neighboring vegetated grid cells (i.e., no longer limited to brush). Scenario D repeats this step upon C twice, and Scenario E repeats 3 additional times upon D. The intermediate scenarios that represent intermediate conditions between C and D (i.e., Scenario C_1), and D and E (i.e., Scenarios D_1, and D_2) are demonstrated in **Figure S6**. To quantify the vegetation cover change relevant to the fire, for each scenario, we calculate the fractional change in the cover of each general fuel/vegetation type within the burnt area of the baseline fire (**Figure 1f)**. Under baseline scenario A, within the simulated burnt area, over half of the area is covered with shrubs (i.e., brush or chaparral). From B to E, the vegetation gradually shifts to a grass-dominated landscape, with increasing grass

coverage in each scenario and resulting in over 60% of the area covered by grass in the most aggressive Scenario E.

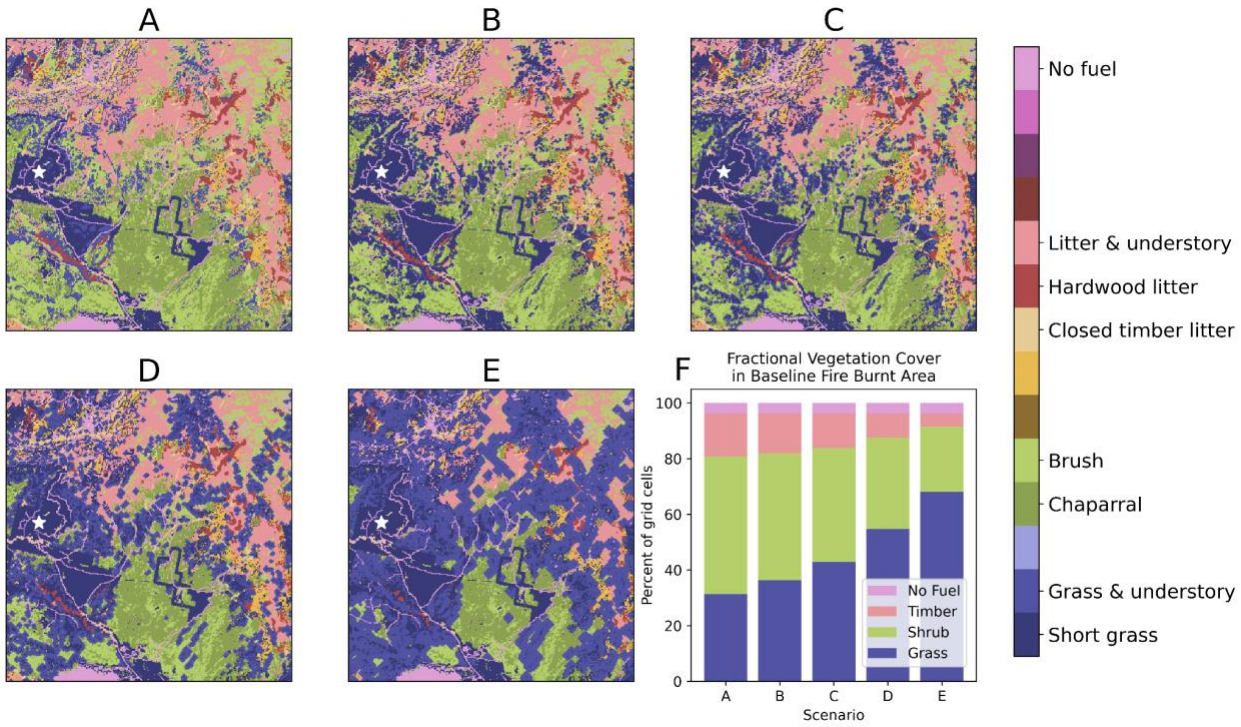

Figure 1. Fuel condition scenarios considered for our simulations of the Mountain Fire. **(a-e)** Maps of fuel category distribution near the ignition point of the Mountain Fire. **(f)** Fractional vegetation cover of each general fuel category over the area burnt in the baseline fire modeled by WRF-Fire (i.e., under fuel condition A).

3 Results

3.1 Evaluation of the baseline simulation

In **Figures 2a** and **2b**, we compare the observed spread of the Mountain Fire to our WRF-Fire simulation under scenario A, the baseline fuel condition in the first 17 hours after igntion. WRF-Fire generally performs well in reproducing the spread of the fire in terms of its

direction and extent. In both the observed and simulated fires, the spread of the Mountain Fire is to the east, driven by westerly winds (**Figure 2a,b**). The simulated fire spread is also consistent with the observations at both ~7 and ~17 hours post-igntion. The overall similarities between the observed and simulated fire perimeters suggest that WRF-Fire can realistically reproduce the Mountain Fire in the baseline condition and can thus be used to explore how this fire may have differed if vegetation characteristics had varied.

We acknowledge that noticeable differences still exist between the observed and simulated fire spreads. The simulated fire spread was slightly slower than observed at ~7 hours post-ignition and somewhat faster and more southward at ~17 hours post-ignition. The differences are largely due to WRF-Fire's limitations in simulating how the fire crosses roads. For example, at ~13.5 hours post-ignition (**Figure 2b**), the fire spread follows roughly the same direction as the observed perimeter. However, as the simulated fire front encounters a road, it eventually crosses not at the observed location but at a location slightly south. **Figure S7** shows how the road-caused deflections in the fire direction are amplified over time.

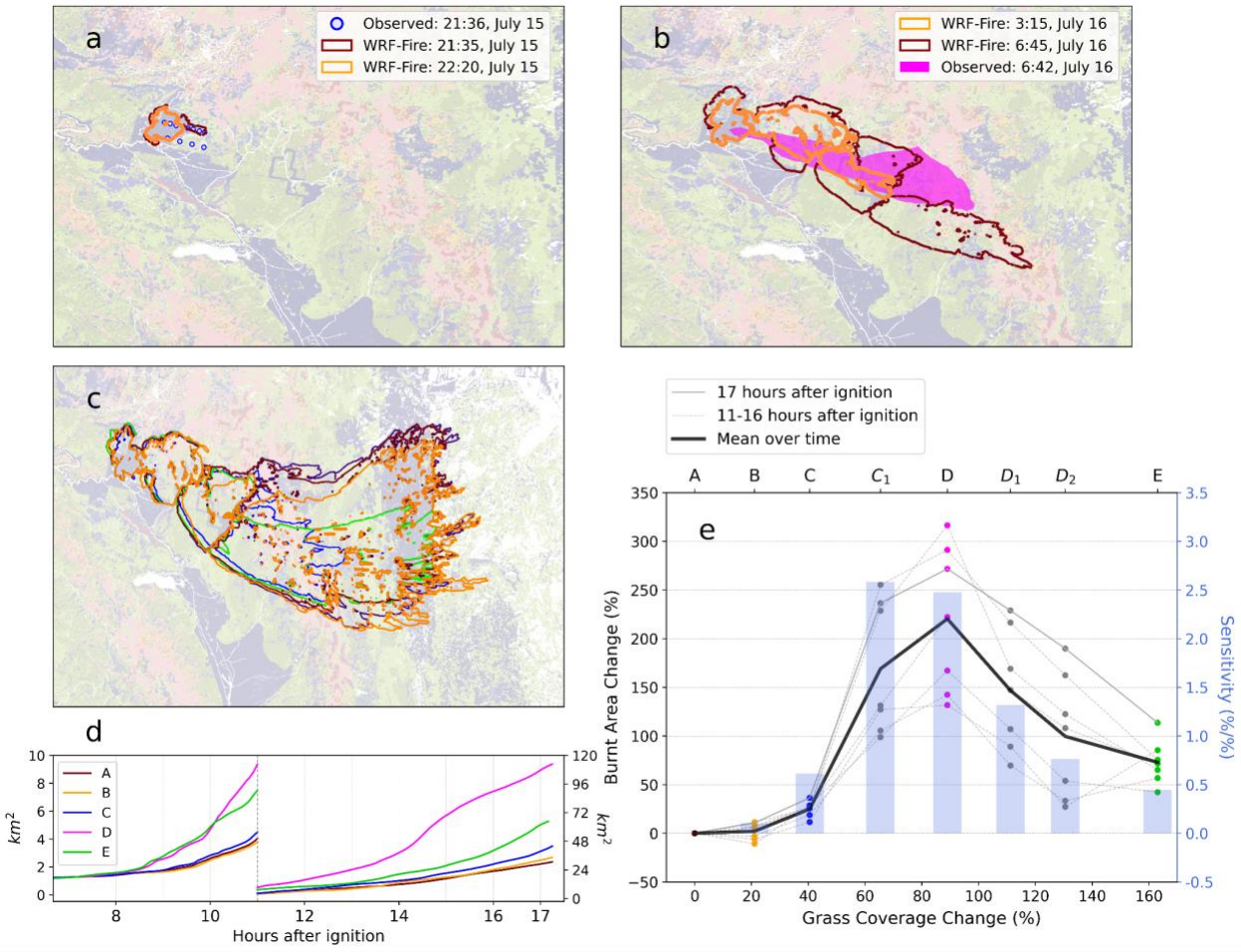

Figure 2. Comparison between **(a)** the observed Mountain Fire and **(b)** WRF-Fire simulated baseline fire burnt area at 21:35, July 15th and 6:45, July 16th, local time. Roads are highlighted in white in **(b)** to demonstrate their impact on the modeled fire spread. **(c)** Simulated fire perimeters 17 hours after ignition under each scenario. **(d)** Simulated burnt area as a function of time since ignition under each scenario. All scenarios have near-identical spread rates before the period shown. To aid visualization, the curves before 11 hours follow the scale on the left; the rest follow the scale on the right. **(e)** Burnt area sensitivity to change in fractional grass coverage

over the last 7 hours of the simulation. The bars show the % increase in burned area (relative to baseline) per each % increase in grass cover.

3.2 Fire spread change under alternative fuel conditions

Using the same model setup, we simulate the Mountain Fire under the alternative fuel scenarios B through E (**Figure 2c**). The 17-hour burned area grows with each incremental increase in grass coverage through scenario D. Relative to Scenario A, the 21% and 41% increases in grass cover in B and C, respectively, result in 11% and 36% increases in the 17-hour fire spread. An 89% grass cover increase in D leads to an outsized 272% increase in burnt area, the largest among all scenarios. Scenario E, with the largest grass cover increase (+163% from A), has a slower fire spread than D (+114% from A) but is still greater than B and C. In the baseline Scenario A, the fire generally spreads along a straight line following the winds. However, with the altered fuel conditions, the additional grasses allow the cone of spread to widen. The final fire perimeters from 8 scenarios (including C_1, D_1, and D_2; **Figure S9**) show that as grass cover gradually expands, the patterns of increase (A to D) and decrease (D to E) in fire spread are consistent.

Figure 2d shows how simulated area burned increases over time under the baseline and idealized fuel conditions. The largest simulated fires, under Scenarios D and E, first diverge from the others at ~8.5 hours after ignition. The two fires eventually also diverge from each other at ~10 hours post-ignition when D starts to spread much more rapidly than E. The fire under Scenario B remains similar to baseline throughout the simulation period, while the fire in C starts to spread noticeably faster at 14-15 hours after ignition. **Figure 2e** summarizes how fire spread in each scenario relates to the fractional increase in grass coverage in the final 7 hours of the

simulation. If the change in fire spread relative to the baseline responds linearly to grass cover change, the dots in **Figure 2e** for a given time should fall on a straight line. However, the large increases in fire spread in the intermediate grass spread scenarios (C_1 and D) and the relatively smaller increases in scenarios with the highest grass coverage suggest that the sensitivity of fire spread to grass coverage is non-linear. When we quantify the sensitivity of change in fire spread to change in grass coverage (i.e., bars of **Figure 2e**), we show that Scenario C_1 has the largest sensitivity despite a slightly slower fire spread than D, and the sensitivity decreases beyond D so much that although the simulated fire in E still spreads much faster than C, the fire-spread-to-grass-change sensitivity in E has become even lower than in C.

3.3 Nonlinear influence of fuel change on the fire-radiation-wind feedback

To explain the non-linear response of fire spread to grass expansion, we investigate how FRP and wind speed associated with the fire evolve under different scenarios. We identify two points in time when simulated fire spread across scenarios diverges (**Figure 2d**). The first is ~8.5 hours after ignition, when spread rates in D and E begin to increase considerably relative to those of A to C. The second is ~10 hours after ignition, when spread rate in D begins to greatly exceed that of E. Both times show a similar divergence in the mean FRP at the fire front (**Figure 3b**), where the fire front is defined at a given time step as grid cells partially but not completely consumed by the fire during that time step.

The mechanisms that drive the divergences are different. The first divergence is initially driven by favorable wind conditions at ~7 hours after ignition that allow the fire in Scenarios D and E to spread across a road it encountered (**Figure S10**), which occurred ~50 minutes later in Scenarios A to C. While such wind conditions may seem coincidental, it is observed in most

scenarios with larger grass coverage (except D_2). Even though all simulated fires show very similar FRP at this time, as explained below, the lower surface roughness of grasses allows for faster winds. In contrast, the second divergence between D and E is initially driven by an increase in FRP in D relative to E at slightly less than 10 hours after ignition (**Figure 3b**), since the fire in D encounters an area covered by mostly chaparral with high fuel load, while the chaparral is replaced by grass in E with less fuel load. The increase in FRP drives an increase in fire-front wind speed within a few minutes (**Figure 3d**). The resulting change in fire spread reflects both processes (**Figure 3f**). In the ~10-minute period when wind speed hasn't yet responded to the radiation, the higher radiative intensity in D alone drives the faster spread in D than in E. However, as wind speed starts to increase in D and decline in E, the spread rate in D continues to increase, while the spread in E quickly falls behind. Since FRP in E becomes significantly lower than in D, the higher wind-to-radiation sensitivity in E cannot offset the reduced radiation.

To explain why the fire in C eventually spreads faster than those in A and B, given a fire of similar radiation, a more expanded grass cover can promote stronger winds. For example, between 11-12 hours post-ignition, the fire-front FRP in Scenario C is slightly yet consistently lower than that in A, the fire-driven wind speed increase is almost identical between A and C. In contrast, between 12-14 hours post-ignition, the fire-front FRP in C is slightly higher than in A, yet the wind becomes significantly stronger in C. More generally, although the overall FRPs across Scenarios A to C are comparable throughout the simulation, the higher sensitivity of winds to radiation due to increased grass cover is what promotes the fires to spread faster from A to C.

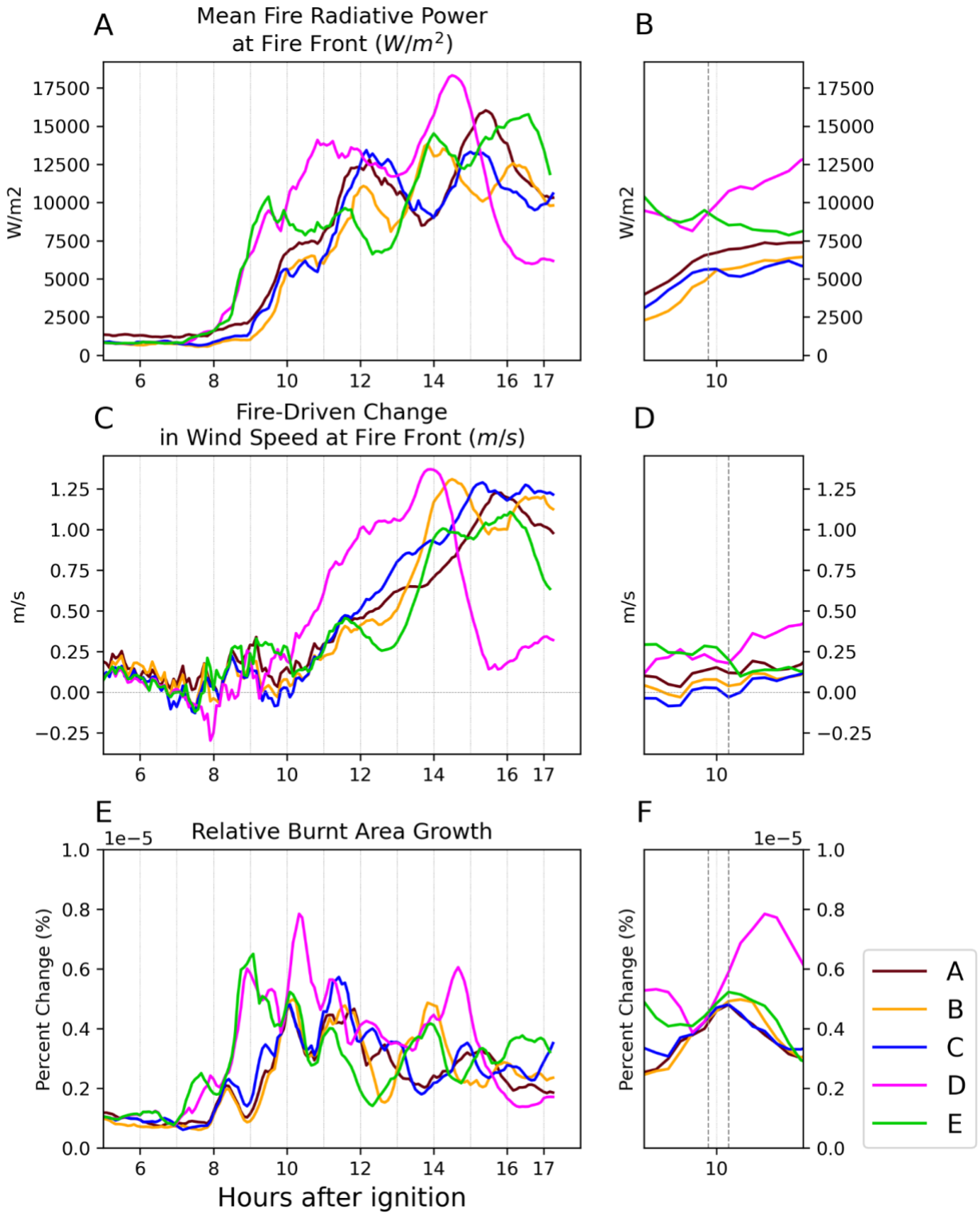

Figure 3. 60-minute rolling mean of the **(a, b)** mean FRP at the fire front, **(c, d)** difference in fire-front wind speed between the with-fire simulations and the background wind speed if no fire

occurred, and **(e, f)** percent increase in each fire's total burnt area in each 5-minute interval under the baseline and alternative fuel conditions. Panels **a, c,** and **e** show the whole time series; **b, d,** and **f** show the time around 10 hours post-ignition. The time corresponds to the end of the moving window.

4 Discussions and Conclusion

Here, we show that the coupled fire-atmosphere model WRF-Fire can simulate how the Mountain Fire would have been affected if grass coverage had been expanded from its observed range at the expense of shrub-dominant vegetation. While our simulations did not represent the specific characteristics of non-native grasses, the scenarios we developed are intended as plausible representations of how invasive grass expansion may affect the vegetation and fuel conditions in Southern California. By creating idealized fuel conditions that represent different extents of grass expansion, we demonstrate that all else held equal (e.g., ignition time and location, meteorological forcing, topography), the expansion of grasses into a predominantly shrub-based vegetation landscape would have induced a more rapidly spreading and intense Mountain Fire. Particularly, as the grass cover progressively expands from the baseline condition to about double its original fraction, the burnt area of the corresponding fire simulation more than triples in our 17-hour simulated period. These results are consistent with previous work using fire simulators and hypothetical invasive grass spread scenarios, which showed how increased invasive grass expansion corresponds to increased fire sizes and burn probabilities (Tortorelli et al., 2023).

We also find that the simulated spread of the Mountain Fire has a highly non-linear response to changes in grass cover due to a fire-radiation-wind feedback. Once grass expansion

causes grass coverage to exceed roughly double its original area, further grass expansion causes the simulated fire spread rate to decline from the peak rate. First, fire spread increases with grass cover primarily because the same FRP released by a fire in a scenario with more grass can generate stronger winds than in a scenario with less grass. This is because grass has a relatively low surface roughness than other vegetation types, allowing for stronger surface winds that promote faster fires. In addition, lower fuel loads in grasses allow for faster burning. Thus, the steady increases in fire spread rates as grass coverage increases incrementally from Scenarios A to C are straightforward to understand. However, the burning of grass leads to less intense fire, as measured by the fire radiative power (FRP), relative to the shrub and forest vegetation types that it replaces in our idealized scenarios. This affects fire spread in two ways. The first is that without considering any feedback with winds, a more intense fire can spread faster. In addition, a weaker FRP generates less atmospheric circulation, and this weakens surface winds. Thus, in the extreme scenario of grass expansion from D to E, the speed-promoting effects of grass in terms of its lower surface roughness and greater potential for rapid consumption begin to be outweighed by the fact that grass burns at a lower intensity than the vegetation types it replaced.

Despite the threshold effect we detect between our most extreme grass-expansion scenarios, all grass-expansion scenarios produce faster fire spread than the baseline scenario, A, which uses the observational land-cover map. Especially under Scenarios D and E with the most pervasive grass spreads, the simulated fires spread significantly faster than the baseline fire partly because toward the end of the simulation, under favorable wind conditions, these two fires spread fast enough to encounter an area of pre-existing, extensive grass cover. This allows the fires in D and E to quickly spread toward the end of the simulation. In the observed Mountain Fire, this grass-covered area was not burned, likely because the wind direction changed before

the observed fire had a chance to reach that area. The inability of the observed fire to spread to the grass area during the period when winds would have led to subsequently rapid expansion may have been aided by fire suppression efforts, which we do not represent in our simulations. It is nonetheless likely that fire suppression would not have been as effective if the fire spread in the initial 8–10 hours had been substantially accelerated due to enhanced grass coverage. Under a condition with a larger grass cover, the faster spreading and larger fire would have led to more serious air pollution and health effects to the downwind population in Palm Springs and beyond.

A limitation of our study of the simulated effects of grass expansion on southern California wildfire is that our simulations were limited to a specific set of meteorological, topographic, and baseline vegetation conditions and it is therefore not known the degree to which our results are generalizable to all fires. For example, it is unclear the degree to which our finding that continued grass expansion will only enhance fire spread rate up to some point before driving further declines in spread rate is generalizable. The conclusion may no longer hold if this method is applied to more fire cases, depending on factors like the meteorological conditions, the dominant vegetation type, and the preexisting fraction of grass cover. Thus, further research is needed to simulate more fires under different climatic and vegetation conditions to better understand the extent to which the conclusions reached in this study are generalizable and the factors that can lead to diverging behaviors across fires. Regardless of these limitations, the outsized influence of invasive grass spread on wildfire spread rates discovered in this study provides valuable insights, especially considering how climate change can create more favorable conditions for invasive grass spread.

Acknowledgments

BW is supported by the UCLA Undergraduate Research Scholars Program. TWJ is supported by the NSF NCAR, which is a major facility sponsored by the U.S. National Science Foundation under Cooperative Agreement No. 1852977, and by the NSF LEAP-HI program (grant number CMMI-1953333). APW is funded by the Gordon and Betty Moore Foundation (#11974) and the John D and Catherine T MacArthur Foundation. We acknowledge computational resources at the NSF NCAR-Wyoming Supercomputing Center provided by the NSF and the State of Wyoming, and supported by NSF NCAR's Computational and Information Systems Laboratory.

Open Research

The WRF-Fire v4.4 code used for the simulations is publicly available on GitHub (https://github.com/wrf-model/WRF/tree/release-v4.4). The ERA5 meteorological forcing is accessed through the NCAR Globally Accessible Data Environment (GLADE) file system. The topographic and fuel input data are available at LANDFIRE (www.landfire.gov).

The NIFC fire perimeter data is accessed at: https://ftp.wildfire.gov/public/incident_specific_data. The VIIRS data is accessed at: https://firms.modaps.eosdis.nasa.gov/download.

5 Supplementary Materials

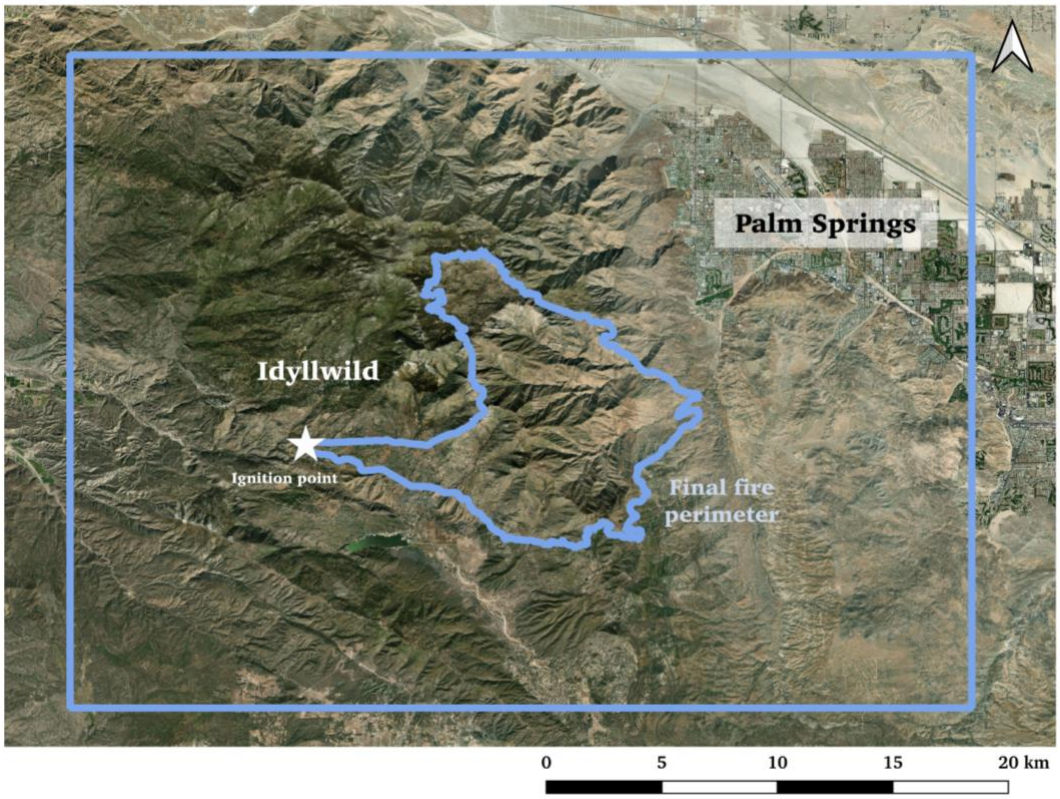

Supplementary Figure 1. Map of the final fire perimeter for the Mountain Fire (2013). The blue square surrounding the fire perimeter is the extent of the innermost domain in the WRF-Fire setup.

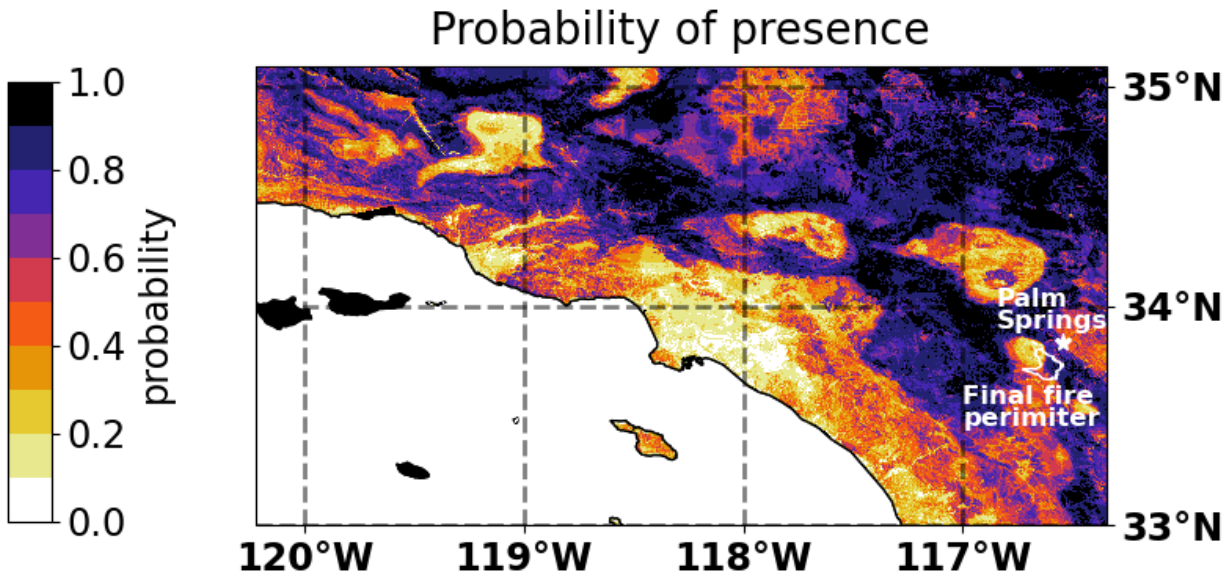

Supplementary Figure 2. Probability of the presence of at least one of the non-native invasive annual grass species—Schismus barbatus (Common Mediterranean grass), Bromus tectorum (Cheatgrass), and Bromus rubens (Red brome) (McMahon et al., 2021) for southern California. The probability of the presence of each species is modeled based on climate, soil, topography, and disturbance records. The maximum probability for each grid cell across the species is shown. The final fire perimeter for the Mountain Fire (2013) is shown in white. The city of Palm Springs is marked with a white star.

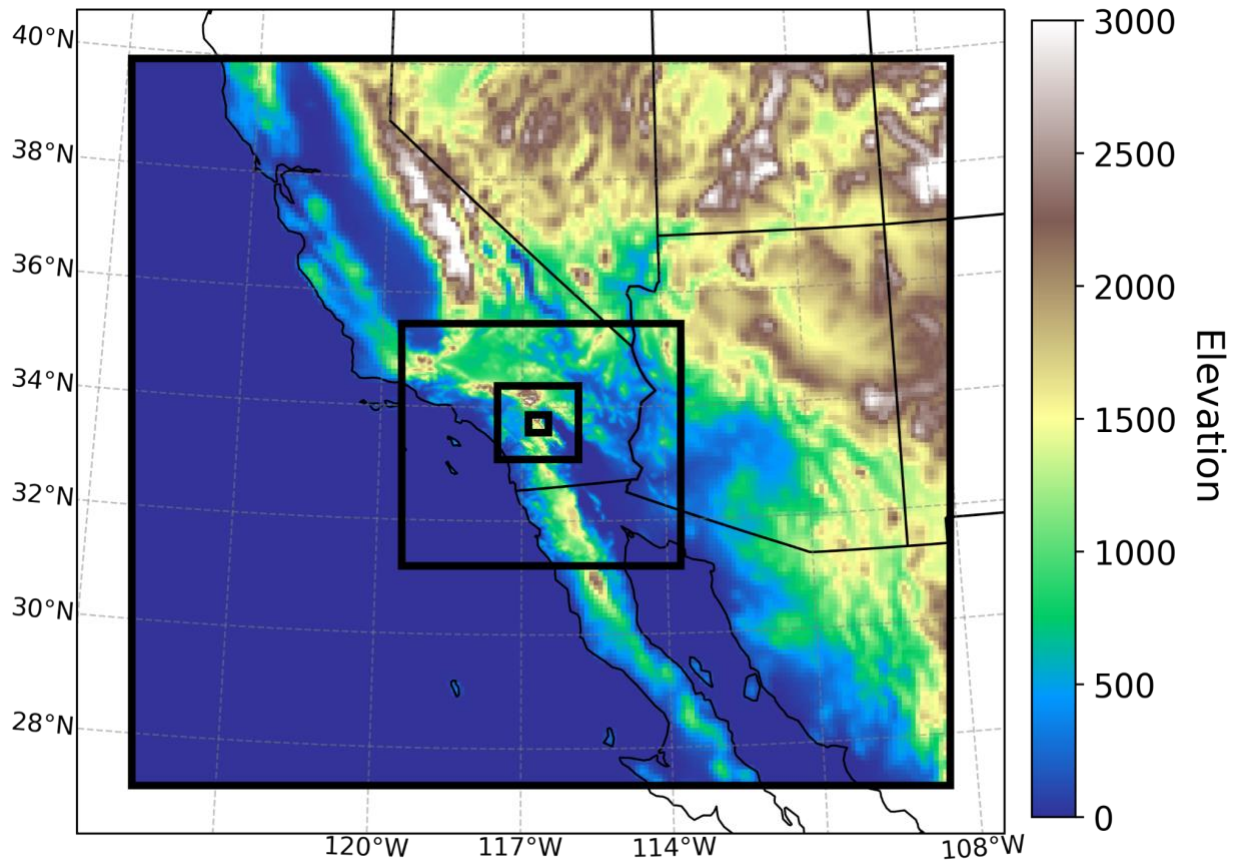

Supplementary Figure 3. WRF-Fire 4-domain setup. Each black box is the boundary for a domain. Horizontal grid cell spacing is 9km, 3km, 600m, and 120m, in the order of outer to inner domain. The colors on the map represent the elevation of each grid cell.

Supplementary Text 1

Key physics schemes used in our simulations include:

the Thompson microphysics scheme (Thompson et al., 2008),

the RRTMG longwave and shortwave schemes (Iacono et al., 2008),

the Eta Similarity Scheme (Janjic, 1994) for the surface layer,

the Noah-MP land surface model (Niu et al., 2011),

and for the planetary boundary layer,

the Mellor–Yamada–Janjic Scheme (MYJ) scheme (Janjic, 1994) for the 3 outer domains,

and the Deardoff subgrid model for the innermost domain.

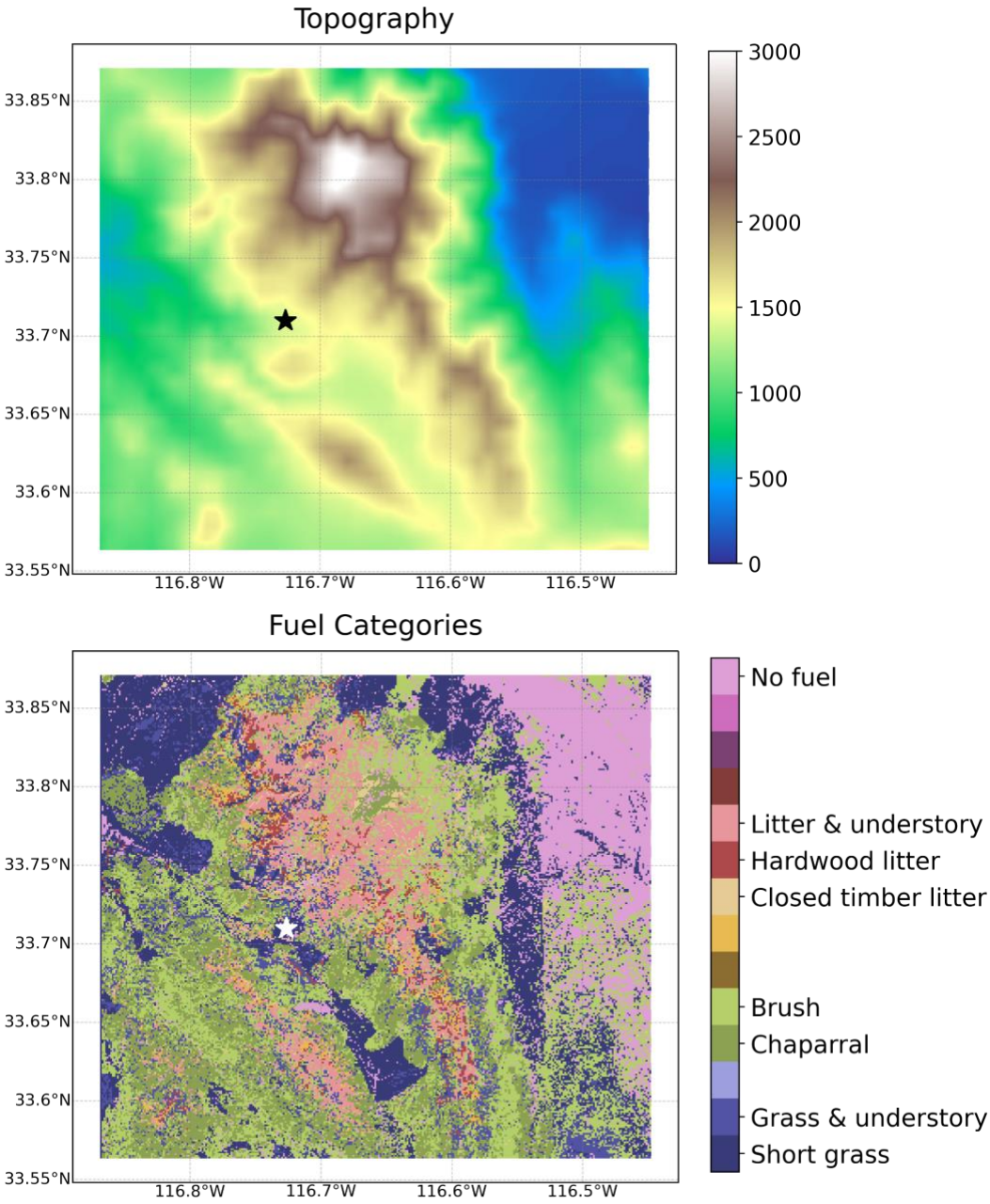

Supplementary Figure 4. Topographic and Anderson-13 fuel category data in the innermost domain from LANDFIRE. The fuel category data is coarsened by sampling every grid cell in every four grid cells. The star in each figure shows the ignition point.

Supplementary Text 2

For wildfires in the wildland-urban interface (WUI) like the Mountain Fire, roads play an important role in shaping directions of, delaying, or even blocking the spread of fires (Juliano et al., 2023). Specifically, the Mountain Fire started near major highways which delayed its spread in its early stage. Since both the fuel data resolution and simulation grid spacing (30 m) are relatively coarse when compared to the width of most roads, the fuel data often represent roads (i.e., no-fuel grids) as discontinuous scatters with gaps in between, which allow fires to easily burn through. For this reason, when using the raw fuel category data from LANDFIRE, WRF-Fire significantly overestimates the initial spread of the Mountain Fire (**Figure S5**). We manually adjust the fuel category input to WRF-Fire so that all roads relevant to the fire are represented as continuous stretches of no-fuel grid cells with no gaps in between.

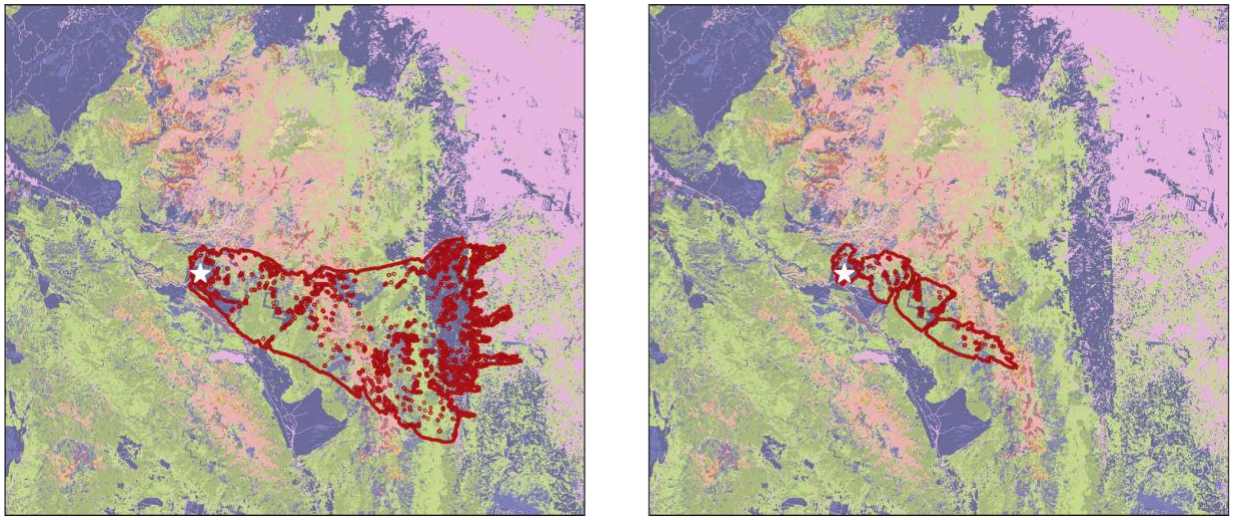

Supplementary Figure 5. Comparison of fire spread between the simulated Mountain Fire ~17 hours after ignition (6:45 am, July 16th, 2013) under **(a)** the raw LANDFIRE fuel map and **(b)** the preprocessed fuel map with roads manually connected.

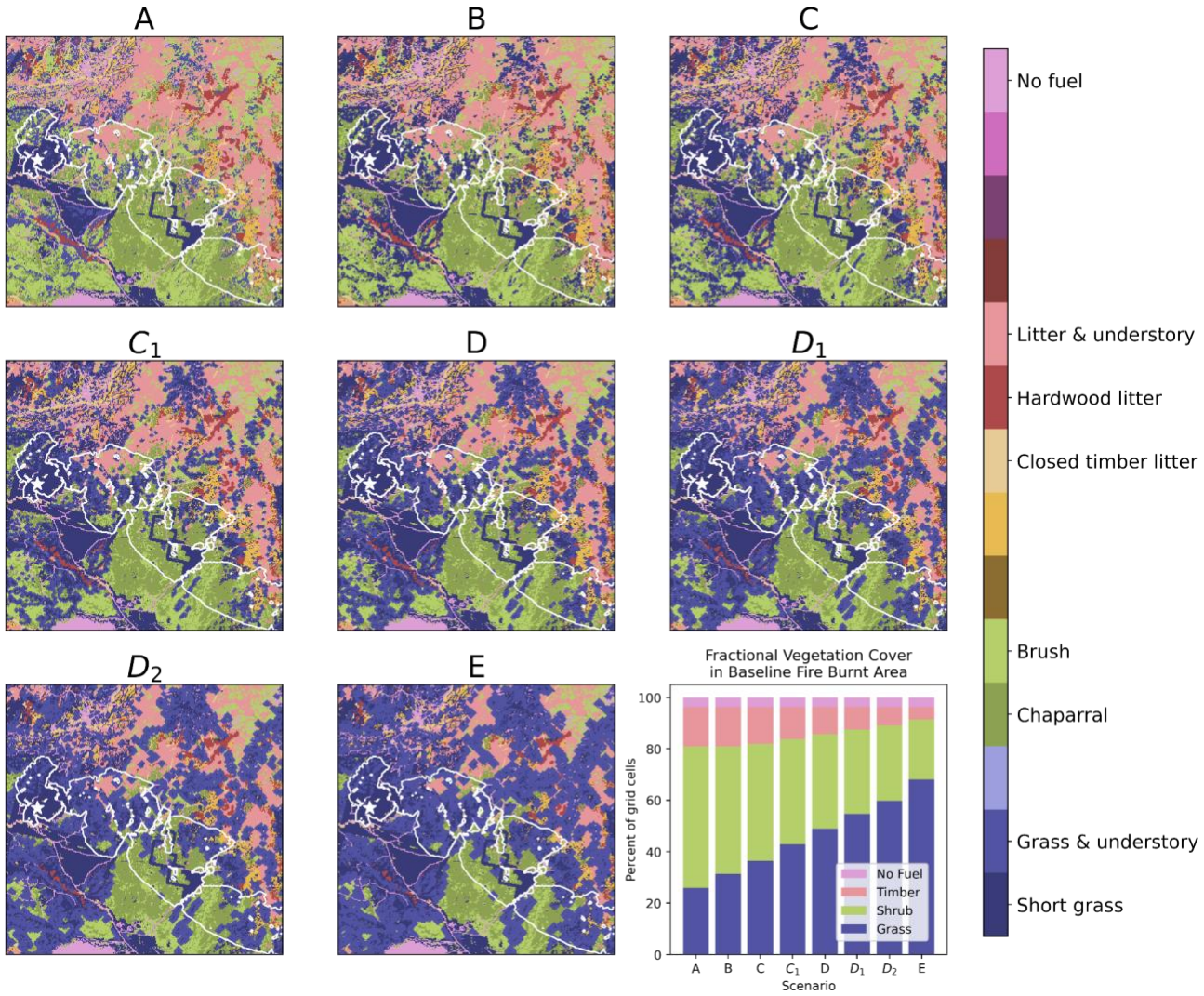

Supplementary Figure 6. Alternative fuel condition schemes for the Mountain Fire. Maps of fuel category distribution near the ignition point of the Mountain Fire, and fractional vegetation cover of each general fuel category over the area burnt in the baseline fire modeled by WRF-Fire (i.e., under fuel condition A). For each scenario from C to E, it is derived by spreading the grass and understory fuel type to the grids that they are immediately neighboring.

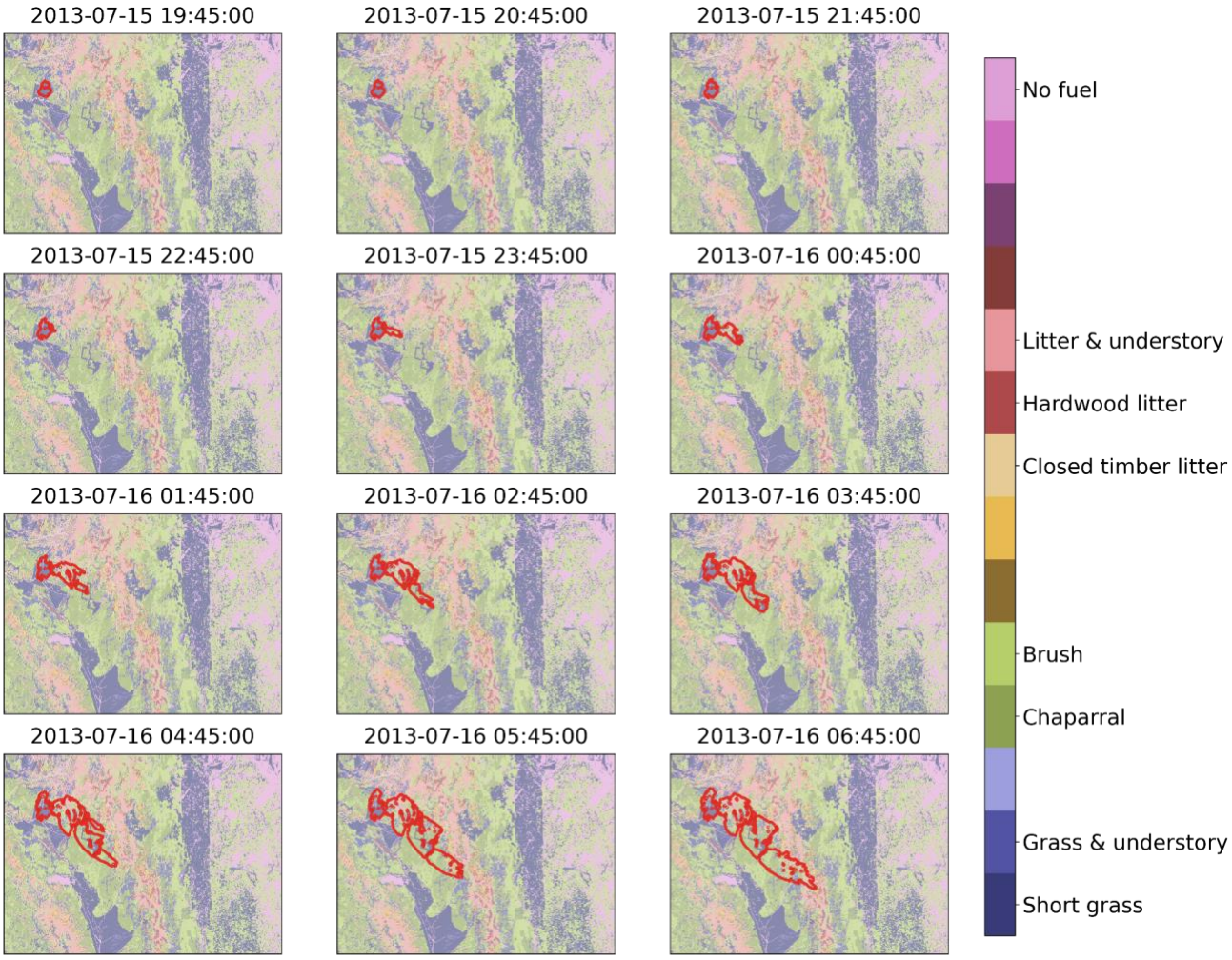

Supplementary Figure 7. Development of the simulated Mountain Fire under the baseline fuel condition.

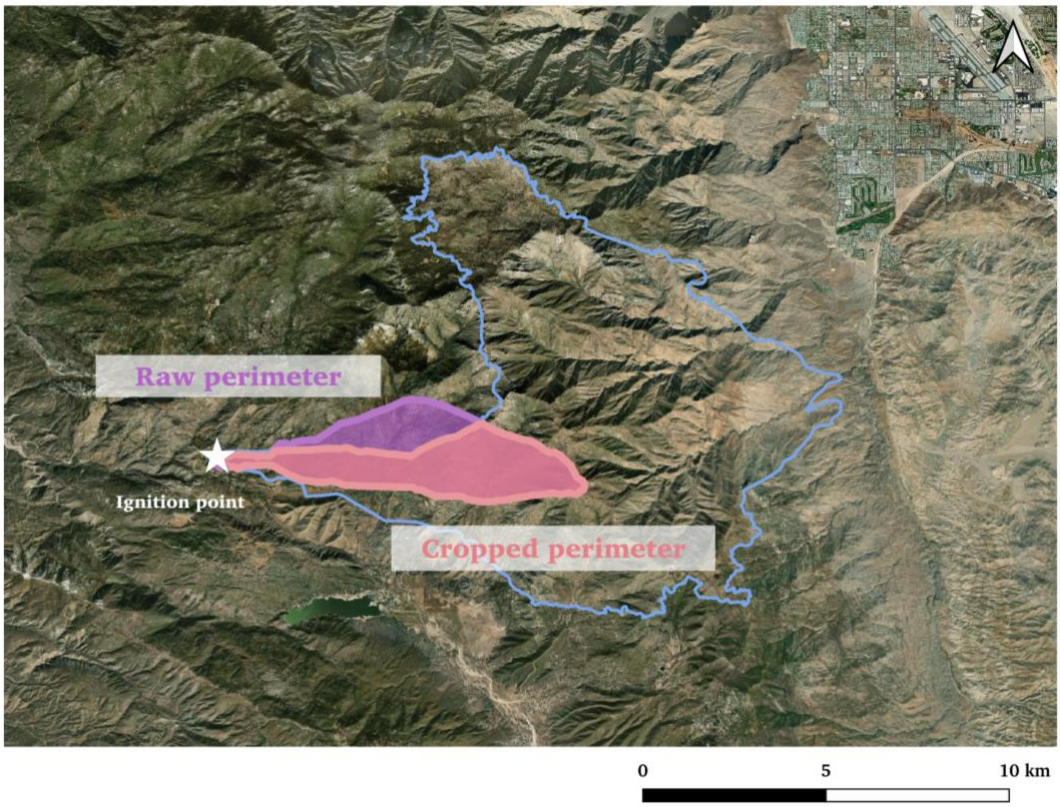

Supplementary Figure 8. Comparison of the raw NIFC fire perimeter at 6:45 am, July 16th and the final fire perimeter. The observed perimeter at 6:45 am, July 16th erroneously covers a portion of the area beyond the fire's final perimeter. Thus, the perimeter shown in **Figure 2a** has the perimeter cropped so that it only covers the area within the final fire perimeter.

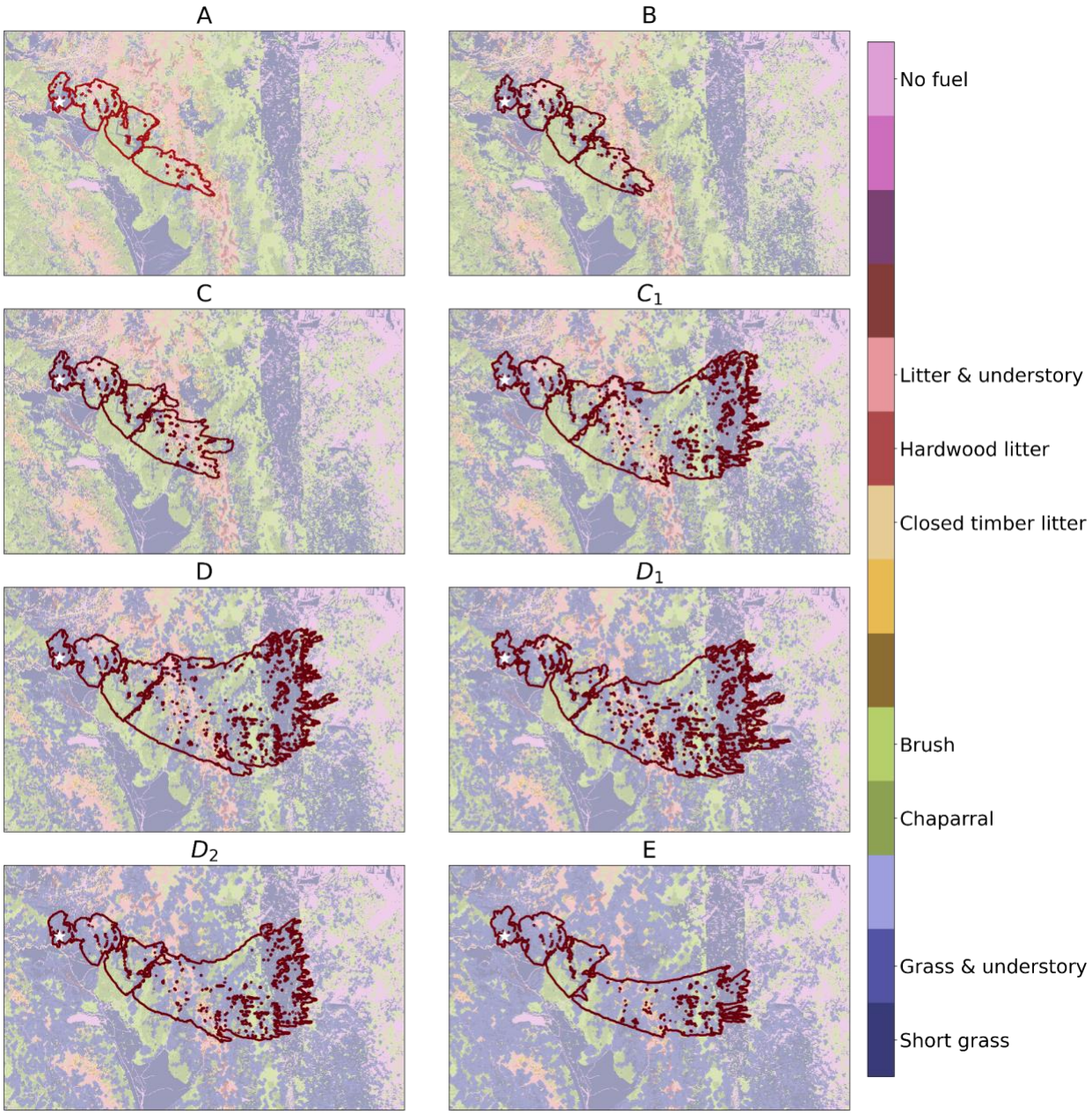

Supplementary Figure 9. Fire perimeters ~17 hours after ignition under all 8 scenarios overlaid on their respective fuel conditions.

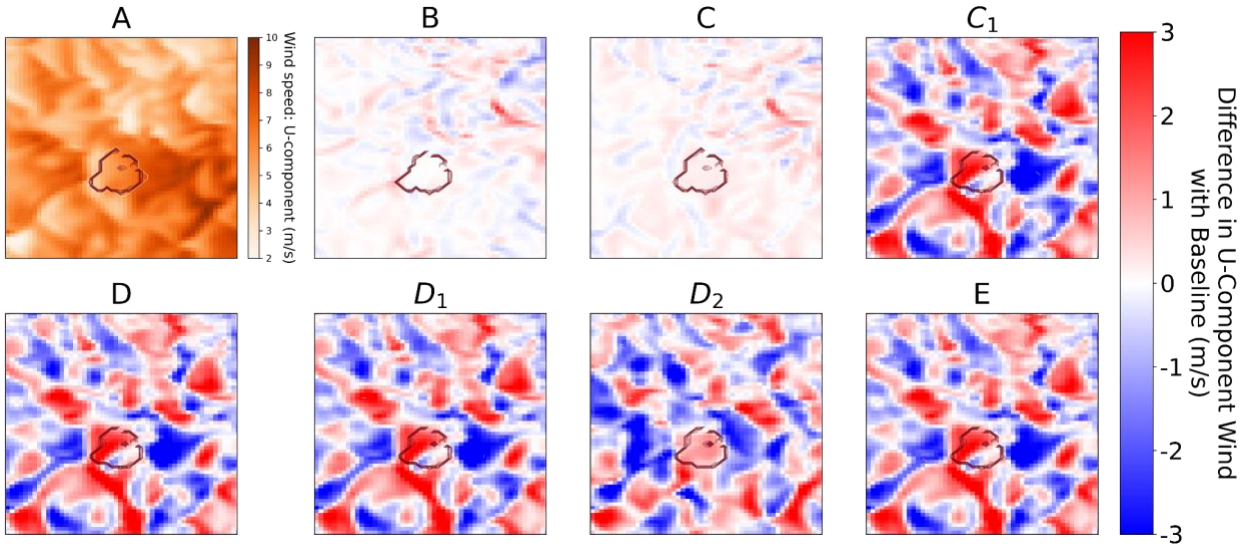

Supplementary Figure 10. U-component wind at ~7 hours after ignition near the fire perimeter. The wind is westerly throughout the demonstrated area. A positive (negative) change indicates a stronger (weaker) westerly wind.

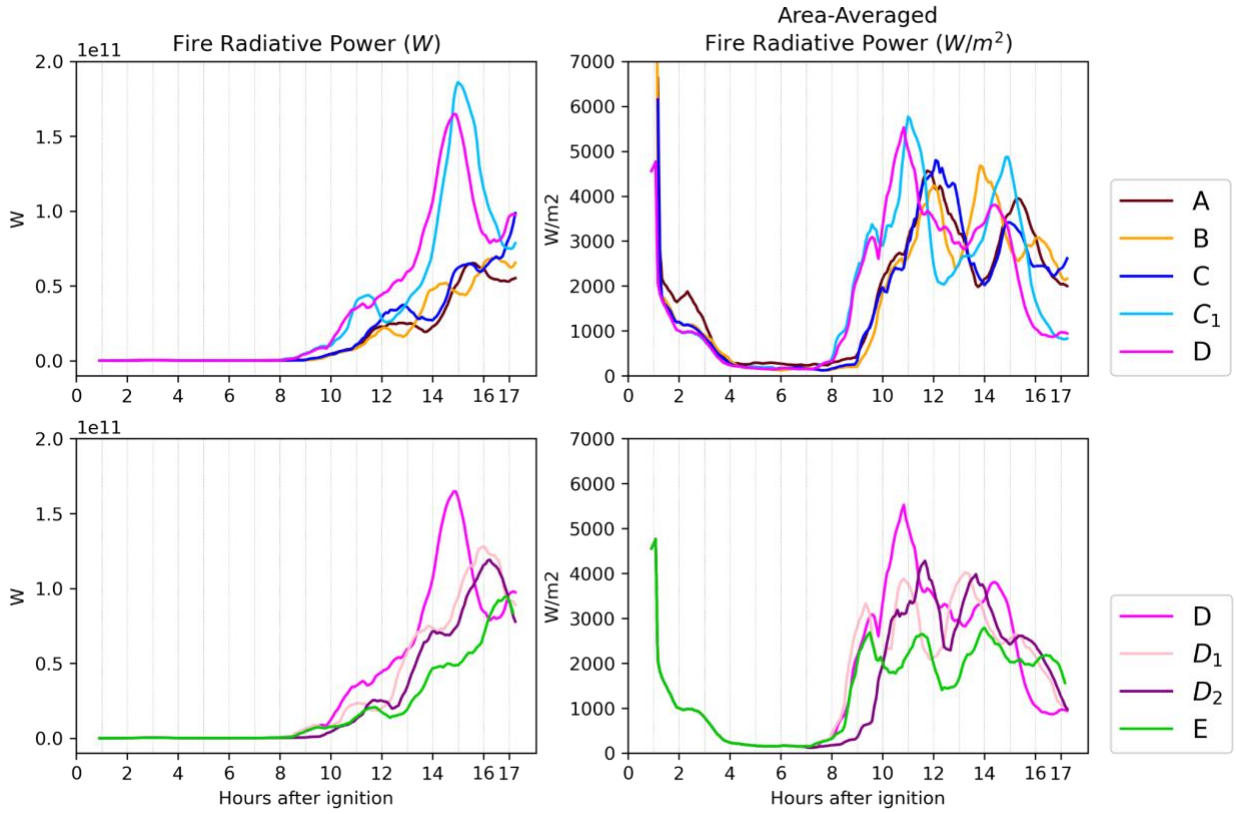

Supplementary Figure 11. 60-minute rolling mean of the **(a, c)** total and **(b, d)** area-averaged WRF-Fire simulated fire radiative power (FRP) under **(a, b)** Scenarios A to D and **(c, d)** Scenarios D to E. The high FRP in Scenarios C_1 and D is consistent with their fastest fire spreads.

References

Abatzoglou, J. T., & Kolden, C. A. (2011). Climate change in western US deserts: Potential for increased wildfire and invasive annual grasses. Rangeland Ecology & Management, 64(5), 471–478. https://doi.org/10.2111/rem-d-09-00151.1

Aguilera, R., Corringham, T., Gershunov, A., & Benmarhnia, T. (2021). Wildfire smoke impacts respiratory health more than fine particles from other sources: observational evidence from Southern California. Nature Communications, 12(1), 1493. https://doi.org/10.1038/s41467-021-21708-0

Anderson, H. E. (1982). Aids to Determining Fuel Models For Estimating Fire Behavior.

Balch, J. K., Bradley, B. A., D'Antonio, C. M., & Gómez-Dans, J. (2013). Introduced annual grass increases regional fire activity across the arid western USA (1980-2009). Global Change Biology, 19(1), 173–183. https://doi.org/10.1111/gcb.12046

Bradley, B. A., Curtis, C. A., Fusco, E. J., Abatzoglou, J. T., Balch, J. K., Dadashi, S., & Tuanmu, M.-N. (2018). Cheatgrass (Bromus tectorum) distribution in the intermountain Western United States and its relationship to fire frequency, seasonality, and ignitions. Biological Invasions, 20.

Brooks, M. L., D'antonio, C. M., Richardson, D. M., Grace, J. B., Keeley, J. E., DiTOMASO, J. M., Hobbs, R. J., Pellant, M., & Pyke, D. (2004). Effects of invasive alien plants on fire regimes. Bioscience, 54(7), 677. https://doi.org/10.1641/0006-3568(2004)054[0677:eoiapo]2.0.co;2

Cocca, C. (2013, July 31). Mountain Fire fully contained after raging for 16 days. NBC Southern California. https://www.nbclosangeles.com/news/local/mountain-fire-fully-contained-after-16-days/2079933/

Coen, J. L., Cameron, M., Michalakes, J., Patton, E. G., Riggan, P. J., & Yedinak, K. M. (2013). WRF-fire: Coupled weather–wildland fire modeling with the Weather Research and Forecasting model. Journal of Applied Meteorology and Climatology, 52(1), 16–38. https://doi.org/10.1175/jamc-d-12-023.1

Corbin, J. D., & D'Antonio, C. M. (2004). Competition between native perennial and exotic annual grasses: Implications for a historical invasion. Ecology, 85(5), 1273–1283. https://doi.org/10.1890/02-0744

D'Antonio, C. M., & Vitousek, P. M. (1992). Biological invasions by exotic grasses, the grass/fire cycle, and global change. Annual Review of Ecology and Systematics, 23(1), 63–87. https://doi.org/10.1146/annurev.es.23.110192.000431

Davies, K. W., & Nafus, A. M. (2013). Exotic annual grass invasion alters fuel amounts, continuity and moisture content. International Journal of Wildland Fire, 22(3), 353. https://doi.org/10.1071/wf11161

Davies, K. W., Leger, E. A., Boyd, C. S., & Hallett, L. M. (2021). Living with exotic annual grasses in the sagebrush ecosystem. Journal of Environmental Management, 288(112417), 112417. https://doi.org/10.1016/j.jenvman.2021.112417

DeCastro, A., Siems-Anderson, A., Smith, E., Knievel, J. C., Kosović, B., Brown, B. G., & Balch, J. K. (2022). Weather research and forecasting—fire simulated burned area and propagation direction sensitivity to initiation point location and time. Fire, 5(3), 58. https://doi.org/10.3390/fire5030058

Donovan, V. M., Wonkka, C. L., Roberts, C. P., Wedin, D. A., McGranahan, D. A., & Twidwell, D. (2023). The influence of wildfire on invasive plant abundance and spatial structure in eastern ponderosa pine savanna. Plant Ecology, 224(11), 987–999. https://doi.org/10.1007/s11258-023-01355-9

Fusco, E. J., Finn, J. T., Balch, J. K., Nagy, R. C., & Bradley, B. A. (2019). Invasive grasses increase fire occurrence and frequency across US ecoregions. Proceedings of the National Academy of Sciences of the United States of America, 116(47), 23594–23599. https://doi.org/10.1073/pnas.1908253116

Hersbach, H., Bell, B., Berrisford, P., Hirahara, S., Horányi, A., Muñoz-Sabater, J., Nicolas, J., Peubey, C., Radu, R., Schepers, D., Simmons, A., Soci, C., Abdalla, S., Abellan, X., Balsamo, G., Bechtold, P., Biavati, G., Bidlot, J., Bonavita, M., … Jean-Noël Thépaut. (2020). The ERA5 global reanalysis. Quarterly Journal of the Royal Meteorological Society. Royal Meteorological Society (Great Britain), 146(730), 1999–2049. https://doi.org/10.1002/qj.3803

Janjić, Z. I. (1994a). The step-mountain eta coordinate model: Further developments of the convection, viscous sublayer, and turbulence closure schemes. Monthly Weather Review, 122(5), 927–945. https://doi.org/10.1175/1520-0493(1994)122<0927:tsmecm>2.0.co;2

Janjić, Z. I. (1994b). The step-mountain eta coordinate model: Further developments of the convection, viscous sublayer, and turbulence closure schemes. Monthly Weather Review, 122(5), 927–945. https://doi.org/10.1175/1520-0493(1994)122<0927:tsmecm>2.0.co;2

Juliano, T. W., Lareau, N., Frediani, M. E., Shamsaei, K., Eghdami, M., Kosiba, K., Wurman, J., DeCastro, A., Kosović, B., & Ebrahimian, H. (2023). Toward a better understanding of wildfire behavior in the wildland-urban interface: A case study of the 2021 Marshall Fire. Geophysical Research Letters, 50(10). https://doi.org/10.1029/2022gl101557

Lipsett, M. J., Tsai, F. C., Roger, L., Woo, M., & Ostro, B. D. (2006). Coarse particles and heart rate variability among older adults with coronary artery disease in the Coachella Valley, California. Environmental Health Perspectives, 114(8), 1215–1220. https://doi.org/10.1289/ehp.8856

McMahon, D. E., Urza, A. K., Brown, J. L., Phelan, C., & Chambers, J. C. (2021). Modelling species distributions and environmental suitability highlights risk of plant invasions in western United States. Diversity & Distributions, 27(4), 710–728. https://doi.org/10.1111/ddi.13232

Mordecai, E. A., Molinari, N. A., Stahlheber, K. A., Gross, K., & D'Antonio, C. (2015). Controls over native perennial grass exclusion and persistence in California grasslands invaded by annuals. Ecology, 96(10), 2643–2652. https://doi.org/10.1890/14-2023.1

Muñoz-Esparza, D., Kosović, B., Jiménez, P. A., & Coen, J. L. (2018). An accurate fire-spread algorithm in the Weather Research and Forecasting model using the level-set method. Journal of Advances in Modeling Earth Systems, 10(4), 908–926. https://doi.org/10.1002/2017ms001108

Rew, L. J., & Johnson, M. P. (2010). Reviewing the role of wildfire on the occurrence and spread of invasive plant species in wildland areas of the intermountain western United States. Invasive Plant Science and Management, 3(4), 347–364. https://doi.org/10.1614/ipsm-08-107.1

Roberts, M., Lareau, N. P., Juliano, T. W., Shamsaei, K., Ebrahimian, H., & Kosovic, A. B. (2023). Sensitivity of Simulated Fire-Generated Circulations to Fuel Characteristics During Large Wildfires. Journal of Geophysical Research Atmospheres.

Sandel, B., & Dangremond, E. M. (2012). Climate change and the invasion of California by grasses. Global Change Biology, 18(1), 277–289. https://doi.org/10.1111/j.1365-2486.2011.02480.x

Shamsaei, K., Juliano, T. W., Roberts, M., Ebrahimian, H., Kosovic, B., Lareau, N. P., & Taciroglu, E. (2023). Coupled fire-atmosphere simulation of the 2018 Camp Fire using WRF-Fire. International Journal of Wildland Fire, 32(2), 195–221. https://doi.org/10.1071/wf22013

Smith, J. T., Allred, B. W., Boyd, C. S., Davies, K. W., Jones, M. O., Kleinhesselink, A. R., Maestas, J. D., Morford, S. L., & Naugle, D. E. (2022). The elevational ascent and spread of exotic annual grass dominance in the Great Basin, USA. Diversity & Distributions, 28(1), 83–96. https://doi.org/10.1111/ddi.13440

Smith, J. T., Allred, B. W., Boyd, C. S., Davies, K. W., Kleinhesselink, A. R., Morford, S. L., & Naugle, D. E. (2023). Fire needs annual grasses more than annual grasses need fire. Biological Conservation, 286(110299), 110299. https://doi.org/10.1016/j.biocon.2023.110299

Thompson, G., Field, P. R., Rasmussen, R. M., & Hall, W. D. (2008). Explicit forecasts of winter precipitation using an improved bulk microphysics scheme. Part II: Implementation of a new snow parameterization. Monthly Weather Review, 136(12), 5095–5115. https://doi.org/10.1175/2008mwr2387.1

Tortorelli, C. M., Kim, J. B., Vaillant, N. M., Riley, K., Dye, A., Nietupski, T. C., Vogler, K. C., Lemons, R., Day, M., Krawchuk, M. A., & Kerns, B. K. (2023). Feeding the fire: Annual grass invasion facilitates modeled fire spread across Inland Northwest forest-mosaic landscapes. Ecosphere (Washington, D.C), 14(2). https://doi.org/10.1002/ecs2.4413

Turney, F. A., Saide, P. E., Jimenez Munoz, P. A., Muñoz-Esparza, D., Hyer, E. J., Peterson, D. A., Frediani, M. E., Juliano, T. W., DeCastro, A. L., Kosović, B., Ye, X., & Thapa, L. H. (2023).

Sensitivity of burned area and fire radiative power predictions to containment efforts, fuel density, and fuel moisture using WRF-fire. Journal of Geophysical Research Atmospheres, 128(18). https://doi.org/10.1029/2023jd038873